Journal of Alloys and Compounds 625 (2015) 90–94

Contents lists available at ScienceDirect

Journal of Alloys and Compounds

journal homepage: www.elsevier.com/locate/jalcom

Letter

Synthesis of 1D Sb_2S_3 nanostructures and its application in visible-light-driven photodegradation for MO

Hulin Zhang [a,*], Chenguo Hu [b], Yong Ding [c], Yuan Lin [a,d,*]

[a] State Key Laboratory of Electronic Thin Film and Integrated Devices, University of Electronic Science and Technology of China, Chengdu, Sichuan 610054, China
[b] Department of Applied Physics, Chongqing University, Chongqing 400044, China
[c] School of Materials Science and Engineering, Georgia Institute of Technology, Atlanta, GA 30332-0245, United States
[d] Institute of Electronic and Information Engineering in Dongguan, University of Electronic Science and Technology of China, Dongguan 523808, Guangdong, China

ARTICLE INFO

Article history:
Received 19 September 2014
Received in revised form 17 October 2014
Accepted 7 November 2014
Available online 15 November 2014

Keywords:
Sb_2S_3
Nanowires
Photocatalytic degradation
MO

ABSTRACT

One-dimensional (1D) antimony trisulfide (Sb_2S_3) nanostructures with different morphologies have been synthesized by a facile hydrothermal and solvothermal method at low temperature, respectively, in the absence of organic dispersant or capping agents. The as-prepared Sb_2S_3 samples were characterized with X-ray diffraction (XRD), scanning electron microscopy (SEM), transmission electron microscopy (TEM) and selected area electron diffraction (SAED), suggesting a single-crystalline orthorhombic structure with 1D morphology. X-ray photoelectron spectrometer (XPS) analysis was performed to study electronic valence states of the as-prepared Sb_2S_3 sample. The band gap of the Sb_2S_3 nanowires can be calculated as about 1.56 eV from the UV–visible reflection spectrum. The photocatalysis of Sb_2S_3 nanowires was investigated by the degradation of methyl orange (MO) under the simulated sunlight, demonstrating the Sb_2S_3 nanowire catalyst has high photocatalytic activity.

1. Introduction

In recent years, investigations on binary chalcogenides of group 15 elements of type, A_2B_3 (A = As, Sb, Bi; B = S, Se, Te) have been paid great attention to scientific researchers owning to their distinctive physical and chemical properties [1–3]. Some of these metallic sulfides with excellent optical and electrical properties can be potentially applied in photovoltaic and thermoelectric devices in the near future [4–6]. Among these binary sulfides, antimony trisulfide (Sb_2S_3) is of particular significance because of its interesting properties and potential technological applications, such as television cameras, solar cells, microwave devices, switching sensors, thermoelectric and optoelectronic devices [7–11]. Moreover, Sb_2S_3 is an important semiconductor material with high photosensitivity and thermoelectric power that crystallizes in the orthorhombic system with the Pnma space group [12,13]. The band gap of Sb_2S_3 is reported at around 1.6 eV [14]. As a result of the narrow band gap, Sb_2S_3 is considered as a promising candidate for solar cells, semiconductor sensors and photovoltaic devices due to that it can widely absorb the visible and near infrared radiation range of the solar energy [1,15]. In addition, semiconductor binary sulfide nanomaterials with various morphologies, which can significantly improve specific surface area [16,17], as well as suitable band gap, are quite possible to apply in photocatalysis, especially in visible-light-driven photodegradation. Nevertheless, photocatalysis based on Sb_2S_3 nanostructures have seldom been reported for MO degradation.

Owning to the aforementioned extensive application, the preparation of Sb_2S_3 nanostructures has been more attractive. Some approaches have been employed to synthesize Sb_2S_3 nanocrystals. Validzic's group has invented a multi-step colloidal reaction to obtain Sb_2S_3 nanocrystals assisted by tetradecanoic acid and butanoic acid [18]. Han and Chen also developed a wet chemical route by the decomposition of $Sb(C_7H_7OCSS)_3$ in N, N-dimethylformamide solution [19]. Lu and coworkers reported a hydrothermal approach with the assistance of polyvinylpyrrolidone for synthesizing Sb_2S_3 nanomaterials [20]. However, these methods are relatively complicated, and involve expensive equipments or toxic chemicals. Still, it is necessary to introduce a simple, low-cost and environmental-friendly method without using any surfactants and templates for the synthesis of Sb_2S_3 nanostructures with high quality at lower temperature.

* Corresponding authors at: State Key Laboratory of Electronic Thin Film and Integrated Devices, University of Electronic Science and Technology of China, Chengdu, Sichuan 610054, China. Tel.: +86 28 83208813 (Y. Lin). Tel.: +86 28 83203901 (H. Zhang).
E-mail addresses: zhangd198710@gmail.com (H. Zhang), linyuan@uestc.edu.cn (Y. Lin).

http://dx.doi.org/10.1016/j.jallcom.2014.11.052
0925-8388/

Table 1
Experimental conditions for the preparation of Sb_2S_3 nanostructures.

Methods	Hydrothermal		Solvothermal	
'S' sources	Thiourea	$Na_2S{\cdot}9H_2O$	Thiourea	$Na_2S{\cdot}9H_2O$
Morphologies	Nanotubes	Nanowires	Nanorods	nanorods

In the present work, we synthesized 1D Sb_2S_3 nanostructures with different morphologies by a facile hydrothermal and solvothermal method at 180 °C, respectively, in the absence of organic dispersant or capping agents. The as-prepared Sb_2S_3 nanostructures were characterized by XRD, SEM, EDS, TEM and XPS. The UV–visible–near infrared reflection spectrum was recorded. Moreover, the photocatalytic activity of the Sb_2S_3 nanocrystal was examined by degradation of MO solution under the simulated sunlight irradiation.

2. Experimental

All of the chemicals of analytical grade, including $SbCl_3$, $(NH_2)_2CS$ (thiourea), $Na_2S{\cdot}9H_2O$, $CO(NH_2)_2$ (urea), and ethylene glycol were purchased from Chongqing Chemical Company and were used without any further purification. In a typical procedure, 0.46 g $SbCl_3$ and 0.228 g thiourea or 0.72 g $Na_2S{\cdot}9H_2O$ were dissolved in 10 mL deionized water, respectively. Then the two solutions were mixed as well as 1 g urea added. After magnetic stirring for 10 min, the mixture was transferred into Teflon-lined autoclave, followed by hydrothermal treatment for 24 h at 180 °C. Afterwards, the autoclave was let cool down naturally. Finally, the product was washed with deionized water and ethanol several times. The Sb_2S_3 nanocrystals were collected by centrifugation and drying in air. When synthesized by a solvothermal method, the Sb_2S_3 nanostructures were obtained in the same steps besides taking ethylene glycol without urea as the solvent. The specific conditions for synthesis of Sb_2S_3 nanostructures via the two routes are comparatively listed in Table 1.

XRD (BDX 3200 with Cu Kα radiation), SEM (TESCAN VEGA II), TEM (TF 30) and XPS (ESCALab MKII X-ray) were performed to systematically characterize the as-prepared Sb_2S_3 nanostructures. An UV–visible Spectrophotometer (Hitachi U-4100) was employed to explore the optical property of Sb_2S_3.

To evaluate the photocatalytic activity of the obtained Sb_2S_3 nanostructures, the degradation of MO was carried out in exposure to the simulated sunlight at room temperature. Specifically, 30 mg of the Sb_2S_3 nanowire catalyst was dispersed in a 100 mL MO solution with the concentration of 11 mg/L. Prior to irradiation, the solution was stirred continuously for 1 h in the dark to ensure the construction of adsorption equilibrium. Subsequently, a simulated sunlight equipment (CHF-XM-500 W) was utilized to illuminate the solution. At a certain time interval, 3 mL suspension was extracted and then centrifuged to remove the Sb_2S_3 catalyst. The change of MO concentration was determined by examining the maximum absorbance using an UV–visible Spectrophotometer mentioned above.

3. Results and discussions

Fig. 1a shows the typical XRD patterns of the as-synthesized products. All the peaks can be well indexed to the orthorhombic phase of the Sb_2S_3 (JCPDS: 42-1393) with the lattice constants of a = 11.23 Å, b = 11.31 Å, c = 3.84 Å, indicating the four Sb_2S_3 nanocrystals synthesized in different procedures are all well-crystallized. The EDS spectrum represented in Fig. 1b confirms the composition of antimony and sulfur (the Si signal comes from the substrate).

To investigate the morphology and size of the Sb_2S_3 samples, the corresponding SEM images are displayed in Fig. 2. Fig. 2a and b, respectively, exhibit the SEM images of the Sb_2S_3 obtained by the hydrothermal method using thiourea and $Na_2S{\cdot}9H_2O$, which reveals uniform tube-like and wire-like structures, respectively. While the Sb_2S_3 synthesized via the solvothermal route using different sulfur sources are shown in Fig. 2c and d, respectively. Both of them indicate a rod-shaped structure. In a word, all the Sb_2S_3 samples prepared here show a 1D morphology, which is illustrated detailedly in Table 1, suggesting that by changing synthesis methods and sources of sulfur, we can produce 1D Sb_2S_3 nanomaterials with different morphologies.

To clearly see the details of structure, TEM was employed to further investigate the Sb_2S_3 nanowires, as is shown in Fig. 3. Fig. 3a displays a TEM image of a single Sb_2S_3 nanowire, indicating that the diameter of the nanowire is about 250 nm. A HRTEM image of the Sb_2S_3 nanowire is shown in Fig. 3b, which illustrates the interplanar distance is 0.51 nm along the corresponding axis by the measurement and calculation. This interplanar distance can be identified as the (120) crystal plane of the orthorhombic Sb_2S_3 (JCPDS: 42-1393). The SAED patterns, displayed in Fig. 3c and d, further imply that the Sb_2S_3 nanowire is single-crystalline and its growth direction is along [001]. This result is consistent with the XRD characterizations.

The XPS analysis was performed to investigate the purity and composition of the as-synthesized Sb_2S_3 nanowires, as depicted in Fig. 4. Fig. 4a shows the typical XPS survey spectrum, indicating no obvious impurities found in the product. The high-resolution spectra of Sb_2S_3 are shown in Fig. 4b and c, which exhibit the photoelectron spectrum of Sb 3d core level and S 2p core level, respectively. The two peaks at 528.6 eV and 538.3 eV can be indexed to the binding energy of Sb $3d_{5/2}$ and $3d_{3/2}$, respectively. The spectrum of S 2p at the binding energy of 160.1 eV corresponds to the S $2p_{3/2}$. All of the obtained binding energy values of Sb 3d and S 2p are in agreement with the reported data [14,21]. The molar ratio of the product for Sb: S is 0.71: 1 by quantification of the integral area for the XPS peaks, which nearly coincides with the results of XRD.

In order to explore the optical property of Sb_2S_3 nanomaterials, Fig. 5 shows the UV–visible reflection spectrum taken on the Sb_2S_3 nanowire film. It can be assumed as an ideal diffuse reflection owning to that the thickness of the Sb_2S_3 nanowire film is much larger than the size of individual crystals. The ratio between the absorption coefficient and scattering factor from the optical diffuse reflec-

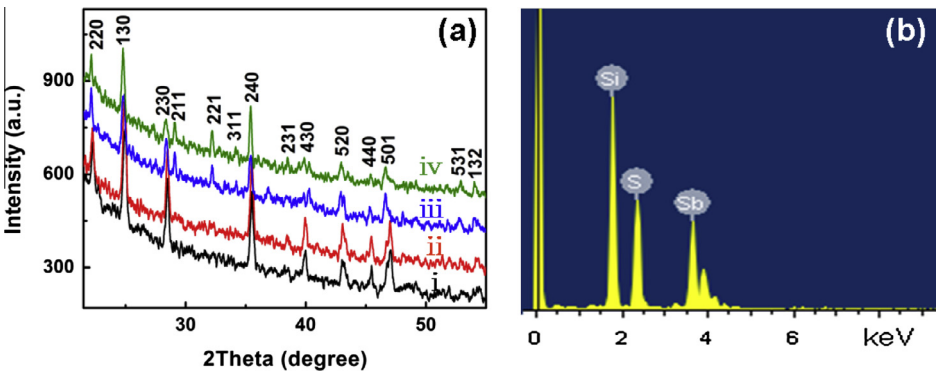

Fig. 1. XRD patterns (a) and EDS (b) of the Sb_2S_3 nanomaterials prepared by the hydrothermal/solvothermal method.

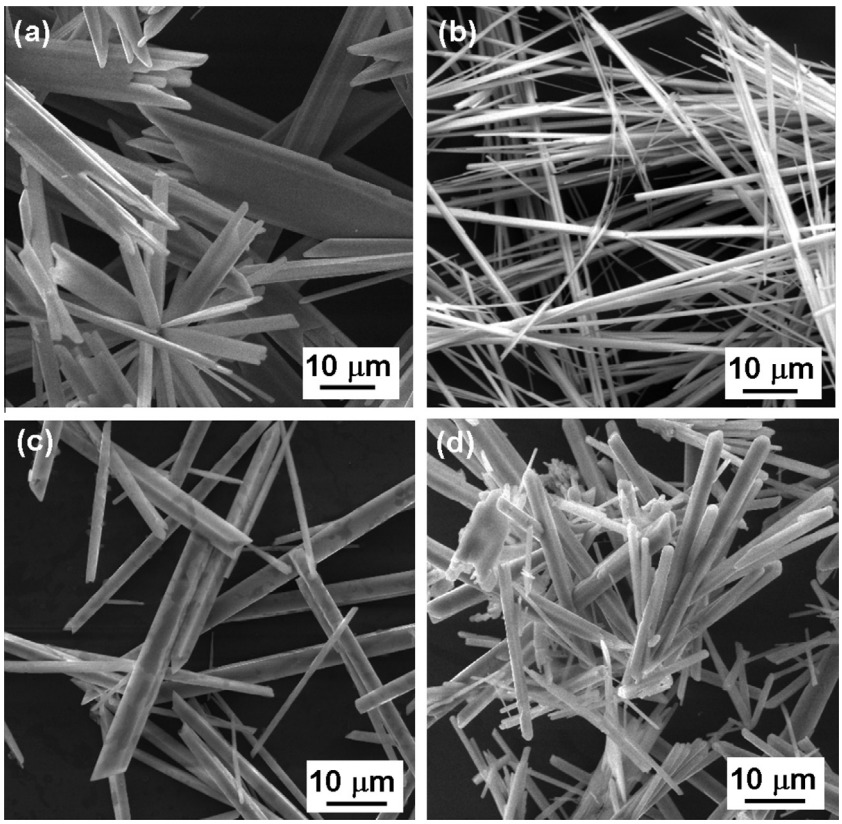

Fig. 2. SEM images of the as-synthesized Sb_2S_3 nanomaterials: (a and b) synthesized by the hydrothermal method with thiourea and $Na_2S{\cdot}9H_2O$, respectively, (c and d) prepared by the solvothermal method with thiourea and $Na_2S{\cdot}9H_2O$, respectively.

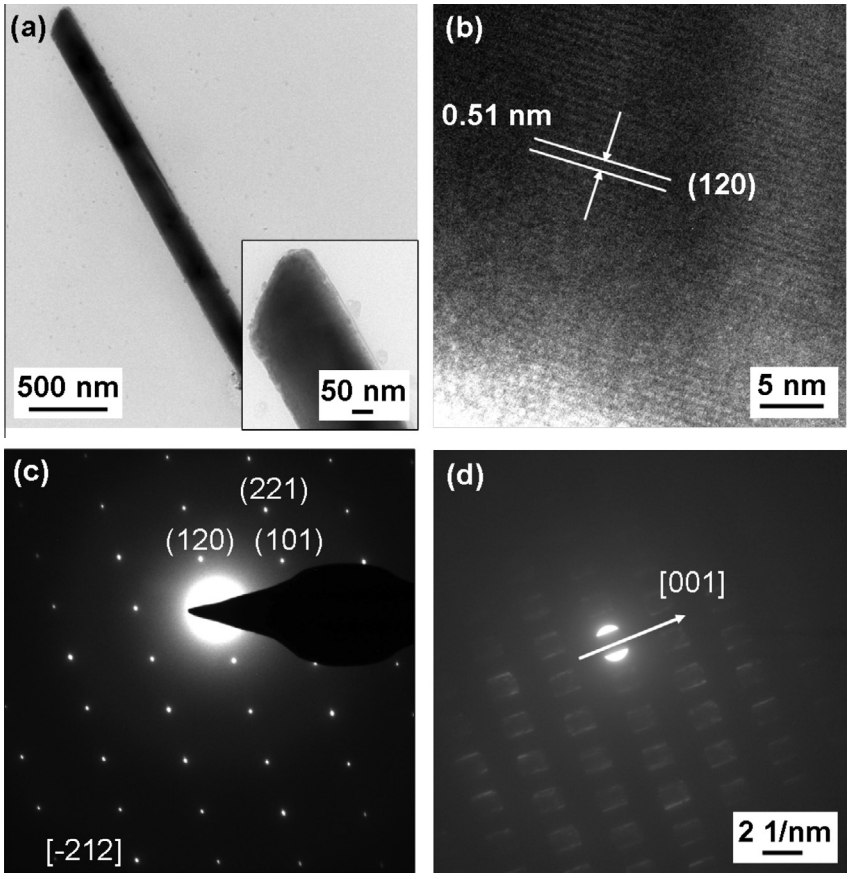

Fig. 3. TEM characterization of the Sb_2S_3 nanowires: (a) TEM image and (inset) the enlarged image, (b) HRTEM image, (c and d) SAED patterns.

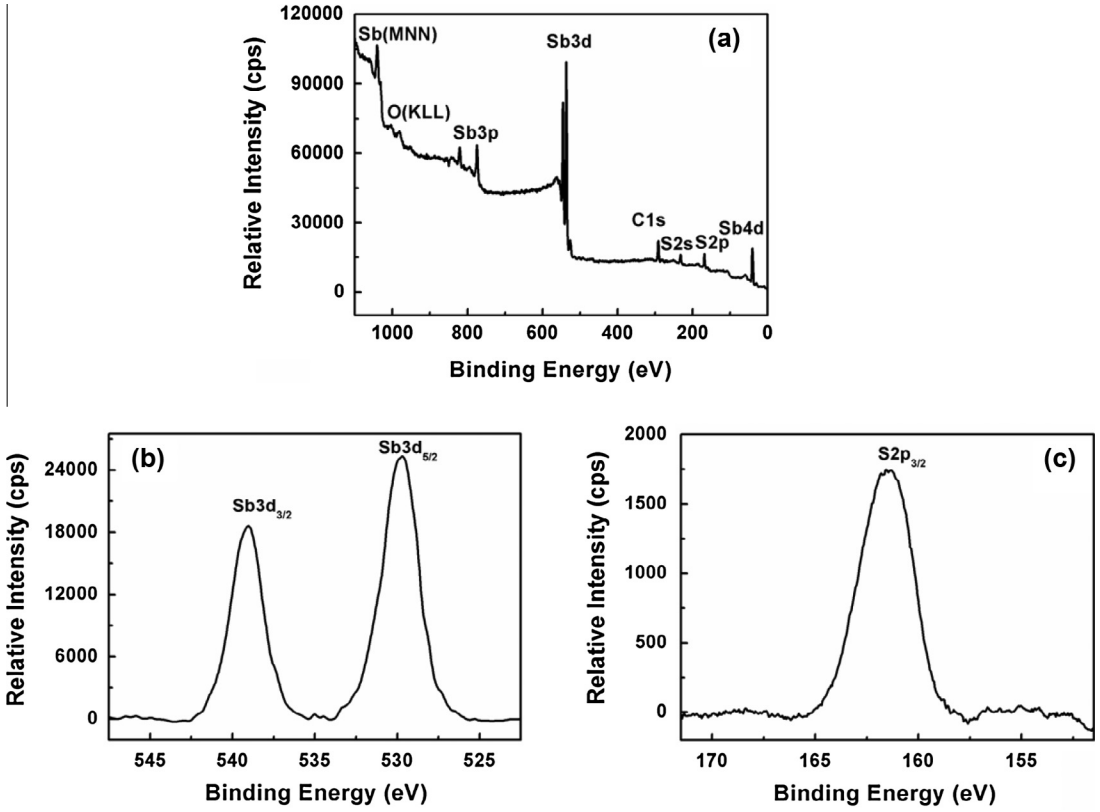

Fig. 4. XPS spectra of Sb_2S_3 products: a typical survey spectrum (a), Sb 3d core level (b), S 2p core level (c).

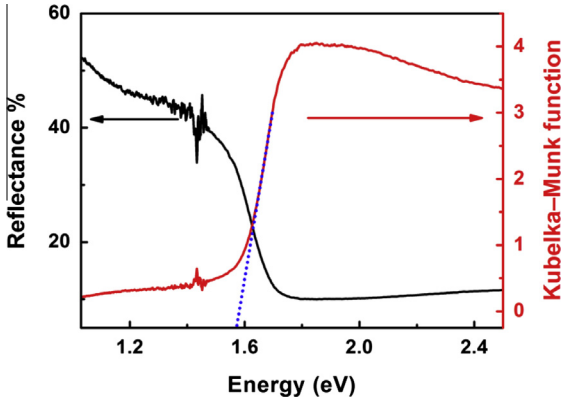

Fig. 5. UV–visible–NIR reflection spectrum and Kubelka–Munk function of the Sb_2S_3 nanowires. Absorption spectra.

tance spectrum [22,23] is defined as the Kubelka–Munk function that is depicted in Fig. 5 based on the recorded diffuse reflectance spectrum. The Kubelka–Munk function is presented below:

$$\alpha = \text{const}(1-R)^2/2R,$$

where α and R are the absorption coefficient and reflectivity, respectively. The function (α/S) can be plotted versus photon energy $(h\nu)$. S is the scattering factor, which can be taken as a constant. By extrapolating the linear part of Kubelka–Munk function, the energy gap of Sb_2S_3 nanowires can be computed as 1.56 eV, in close proximity to the reported results of previous literatures [14,24]. In addition, it is can be noted that the optical absorption nearly covers all of the visible light range, illustrating that the as-synthesized Sb_2S_3 nanowires can be excited by visible light.

To exploit the potential application of Sb_2S_3 nanocrystals, the visible-light-driven photocatalytic degradation was carried out. MO, as a typical organic dye widely existed in industrial waste water, was used for catalytic decomposition under the simulated sunlight with the intensity of 97 mW/cm^2. The degradation process was monitored by recording the absorbance spectra of the MO aqueous solution. The concentration change of MO was estimated based on the characteristic absorption peak of MO centered at 464 nm. Fig. 6 shows the UV–visible absorption spectra of the MO solution for photocatalytic degradation on the Sb_2S_3 nanowires under simulated sunlight at different stages. In the early stage about 1.6% of MO is degraded by stirring in the dark with the Sb_2S_3 nanowires due to the adsorption of nanostructures to organic dyes. It can be found that the concentration of MO declines with the irradiation time, implying that the Sb_2S_3 nanowires show high photocatalytic activity. After 2.5 h illumination, about 71% of MO was catalyzed by the Sb_2S_3 nanowire catalyst, as is plotted in Fig. 6b, further demonstrating that MO can be effectively degraded by the visible-light photocatalysis of the Sb_2S_3 nanowires.

The basic photocatalytic principle is proposed, which relies on the photogenerated electrons (e^-) and holes (h^+) (when irradiation energy is equal to or higher than its band gap). The electrons and holes react with the adsorbed surface substances, like O_2 and OH^-, to form reactive species O_2^-, OH^*, which is the major oxidative species for the decomposition of organic pollutants. Then the oxidative species degrade the organic pollutant (MO) into the small molecules like CO_2 and H_2O [25].

The possible photocatalytic reaction is proposed as follows:

$$Sb_2S_3 + h\nu(E > E_g) \rightarrow Sb_2S3 + h^+ + e^-, \quad (1)$$

$$h^+ + H_2O/OH^- \rightarrow OH^*(+H^+), \quad (2)$$

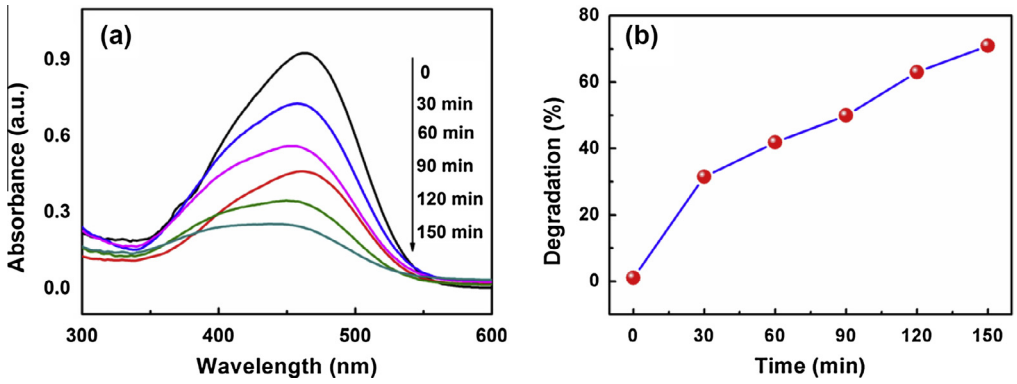

Fig. 6. Monitoring of photodegradation: (a) absorption spectrum of 11 mg/L MO solution with 0.3 g/L Sb_2S_3 nanowire catalyst in different stages under illumination of the simulated sunlight and (b) the plot of degradation percentage versus illumination time.

$$e^- + O_2 \rightarrow O^{2-}, \quad (3)$$

$$OH^*/O^{2-} + MO \rightarrow CO_2 + H_2O + \text{inorganic ion}. \quad (4)$$

The degradation of the organic pollutants is achieved via series of parallel and consecutive redox reactions in Eqs. (2)–(4).

The favourable photocatalytic activity of the Sb_2S_3 nanowires can be attributed to its wide absorption range of visible light, as a result of the narrow band gap. 1D Sb_2S_3 nanowires with larger specific surface area can facilitate the electrons generated by the light transfer between the catalyst interfaces. Hence, the efficiency of photocatalysis improves due to that the probability of the electron–hole recombination decreases. In addition, it is considered that the catalytic activity can be promoted by the larger specific surface area of catalysts because of the less steric hindrance for the diffusion of reactants [26], leading to providing photocatalyst with more total active sites for interaction with holes (or electrons) to form species that degrade organic molecules, which can eventually lead to the decomposition of organic pollutants [27].

4. Conclusions

The 1D Sb_2S_3 nanostructures with different morphologies have been successfully synthesized by a facile hydrothermal and a solvothermal method, respectively. These approaches are simple, easy to scale-up, cost-effective and without using surfactants. The as-prepared Sb_2S_3 nanocrystals are uniform and are characterized systematically. The photocatalytic activity of Sb_2S_3 nanowires was investigated by the degradation of MO under the simulated sunlight. The Sb_2S_3 nanowire catalyst shows high photocatalysis mainly due to its wide absorption range of visible light. Our investigation demonstrates that Sb_2S_3 nanostructures can be potentially utilized in degradation of organic contaminants.

Acknowledgments

This work was supported by the National Basic Research Program of China (973 Program) under Grant No. 2015CB351905, Natural Science Foundation of China (No. 51172036), and the Guangdong Innovative Research Team PNatural Science Foundation of Chinarogram (No. 201001D0104713329).

References

[1] O. Savadogo, K.C. Mandal, Sol. Energy Mater. Sol. Cells 26 (1992) 117–136.
[2] B.B. Nayak, H.N. Acharya, G.B. Mitra, B.K. Mathur, Thin Solid Films 105 (1983) 17–24.
[3] S.H. Pawar, P.N. Bhosale, M.D. Uplane, S. Tamhankar, Thin Solid Films 110 (1983) 165–170.
[4] D. Arivuoli, F.D. Gnanam, P. Ramasamy, J. Mater. Sci. Lett. 7 (1988) 711–713.
[5] B. Chen, C. Uher, Chem. Mater. 9 (1997) 1655–1658.
[6] R. Suarez, P.K. Nair, P.V. Kamat, Langmuir 14 (1998) 3236–3241.
[7] D. Cope, US patent No. 2875 (1959) 359.
[8] K.Y. Rajpure, C.H. Bhosale, Mater. Chem. Phys. 64 (2000) 70–74.
[9] J. Grigas, J. Meshkauska, A. Orliukas, Phys. Status Solidi (a) 37 (1976) K39–K41.
[10] L. Wu, H.Y. Xu, Q.F. Han, X. Wang, J. Alloys Comp. 572 (2013) 56–61.
[11] I.H. Kim, Mater. Lett. 43 (2000) 221–224.
[12] B. Roy, B.R. Chakraborty, R. Bhattacharya, A.K. Dutta, Solid State Commun. 25 (1978) 937–940.
[13] X.W. Zheng, Y. Xie, L.Y. Zhu, X.C. Jiang, Y.B. Jia, W.H. Song, Y.P. Sun, Inorg. Chem. 41 (2002) 455–461.
[14] Q.F. Han, S.S. Sun, D.P. Sun, J.W. Zhu, X. Wang, RSC Adv. 1 (2011) 1364–1369.
[15] M.T.S. Nair, Y. Pena, J. Campos, V.M. Garcia, P.K. Nair, J. Electrochem. Soc. 145 (1998) 2113–2120.
[16] P.C. Wu, Y. Dai, T. Sun, Y. Ye, H. Meng, X.L. Fang, B. Yu, L. Dai, ACS Appl. Mater. Interfaces 3 (2011) 1859–1864.
[17] H.X. Xie, W.X. Que, Z.L. He, P. Zhong, Y.L. Liao, G.F. Wang, J. Alloys Comp. 550 (2013) 314–319.
[18] I.L. Validzic, M. Mitric, N.D. Abazovic, B.M. Jokic, A.S. Milosevic, Z.S. Popovic, F.R. Vukajlovic, Semicond. Sci. Technol. 29 (2014) 035007.
[19] Q.F. Han, L. Chen, M.J. Wang, X.J. Yang, L.D. Lu, X. Wang, Mater. Sci. Eng. B 166 (2010) 118–121.
[20] Q.F. Lu, H.B. Zeng, Z.Y. Wang, X.L. Cao, L.D. Zhang, Nanotechnology 17 (2006) 2098–2104.
[21] J. Ota, S.K. Srivastava, Cryst. Growth Des. 7 (2007) 343–347.
[22] W.M. Wesley, G.H.H. Wendlandt, Reflectance Spectroscopy, Interscience Publishers, John Wiley, New York, 1966.
[23] J. Li, Z. Chen, X.X. Wang, D.M. Proserpio, J. Alloys Comp. 262 (1997) 28–33.
[24] G.Y. Chen, B. Deng, G.B. Cai, T.K. Zhang, W.F. Dong, W.X. Zhang, A.W. Xu, J. Phys. Chem. C 112 (2008) 672–679.
[25] H.L. Zhang, C.G. Hu, Catal. Commun. 14 (2011) 32–36.
[26] Q.Q. Wang, B.Z. Lin, B.H. Xu, X.L. Li, Z.J. Chen, X.T. Pian, Microporous Mesoporous Mater. 130 (2010) 344–351.
[27] T.K. Jia, W.M. Wang, F. Long, Z.Y. Fu, H. Wang, Q.J. Zhang, J. Phys. Chem. C 113 (2009) 9071–9077.